JACS
JOURNAL OF THE AMERICAN CHEMICAL SOCIETY
Article
pubs.acs.org/JACS

Small Gold Nanoparticles Interfaced to Electrodes through Molecular Linkers: A Platform to Enhance Electron Transfer and Increase Electrochemically Active Surface Area

Samantha L. Young,[†] Jaclyn E. Kellon,[†] and James E. Hutchison*

Department of Chemistry and Biochemistry and Materials Science Institute, 1253 University of Oregon, Eugene, Oregon 97403-1253, United States

Supporting Information

ABSTRACT: For the smallest nanostructures (<5 nm), small changes in structure can lead to significant changes in properties and reactivity. In the case of nanoparticle (NP)-functionalized electrodes, NP structure and composition, and the nature of the NP-electrode interface have a strong influence upon electrochemical properties that are critical in applications such as amperometric sensing, photocatalysis and electrocatalysis. Existing methods to fabricate NP-functionalized electrodes do not allow for precise control over all these variables, especially the NP-electrode interface, making it difficult to understand and predict how structural changes influence NP activity. We investigated the electrochemical properties of small (d_{core} < 2.5 nm) gold nanoparticles (AuNPs) on boron doped diamond electrodes using three different electrode fabrication techniques with varying degrees of nanoparticle-electrode interface definition. Two methods to attach AuNPs to the electrode through a covalently bound molecular linker were developed and compared to NP-functionalized electrodes fabricated using solution deposition methods (drop-casting and physiadsorption of a monolayer). In each case, a ferrocene redox probe was tethered to the AuNP surface to evaluate electron transfer through the AuNPs. The AuNPs that were molecularly interfaced with the electrode exhibited nearly ideal, reproducible electrochemical behavior with narrow redox peaks and small peak separations, whereas the solution deposited NPs had broader redox peaks with large peak separations. These data suggest that the molecular tether facilitates AuNP-mediated electron transfer. Interestingly, the molecularly tethered NPs also had significantly more electrochemically active surface area than the solution deposited NPs. The enhanced electrochemical behavior of the molecularly interfaced NPs demonstrates the significant influence of the interface on NP-mediated electron transfer and suggests that similar modified electrodes can serve as versatile platforms for studies and applications of nanoparticles.

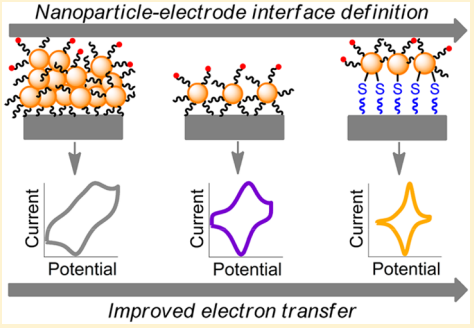

INTRODUCTION

Nanoparticles (NPs) have been employed in a wide range of applications including sensing,[1,2] energy storage and conversion,[3,4] catalysis,[5] and electrochemical applications[6] due to their core size dependent properties and high surface area to volume ratio. NPs can impart chemical reactivity to otherwise inert, but abundant, materials and dramatically increase the surface area available for chemical transformations while minimizing the use of the active, often precious, metals.[7−9]

Nanoparticle-functionalized electrodes have been studied for electrochemical applications such as amperometric sensing,[10,11] photocatalysis,[12] and electrocatalysis.[4,13] In electrochemical applications, the addition of nanoparticles to an electrode surface enhances the electrode's catalytic activity[4,6] and can promote electron transfer through otherwise insulating molecules.[14,15] The enhanced electrochemical properties of NP-functionalized electrodes have been attributed to the NP's electronic structure,[16] surface chemistry,[17] crystal facets,[18−21] density on the electrode surface,[22,23] as well as the interface between the NP and the electrode support.[24−27]

A number of studies have attempted to correlate the electrochemical properties of NP-functionalized electrodes with nanoparticle composition and structure.[13,16,18,28−30] Nanostructures deposited by vacuum evaporation or electrodeposition,[31−33] and their interfaces with the electrode, are difficult to characterize, making it challenging to attribute observed electrochemical properties to specific structures. Such deposition methods also make it hard to control the resulting NP core size distribution or coverage on the electrode. In order to understand the electrochemical properties of specific nanoparticle structures, it is necessary to fabricate NP-functionalized electrodes with uniform NP core sizes, known surface chemistry, and a defined interface between the NP and the electrode support.

The solution deposition of preformed nanoparticles is an alternative strategy to fabricate NP-functionalized electrodes that allows for more rigorous characterization of the NPs since solution-state characterization techniques are available in

Received: July 25, 2016
Published: September 28, 2016

DOI: 10.1021/jacs.6b07674
J. Am. Chem. Soc. 2016, 138, 13975−13984

Scheme 1. Methods of Attaching Preformed, Ligand-Stabilized Nanoparticles to Electrode Substrates

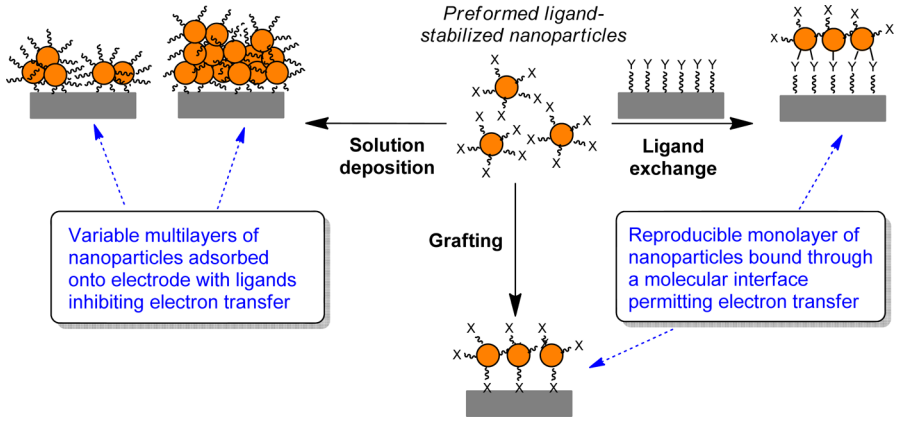

addition to solid-state techniques.[34] Further, bonding such NPs to an electrode might be useful to control the NP-electrode interface. Several methods to deposit (or attach) ligand-stabilized NPs on electrode materials are presented in Scheme 1. The simplest approaches involve solution deposition techniques (e.g., drop-casting, spin-coating, dip-coating) to modify the electrode surface with preformed NPs, or mixing nanoparticles with a support material (i.e., carbon black), which is then fabricated into an electrode.[18,28] While these methods are admittedly convenient, there are several drawbacks making it difficult to directly relate NP morphology to observed electrochemical behavior. Solution deposition methods offer limited control of the NP surface coverage, the NP-electrode interface and/or interactions between the NPs, all of which influence electrochemical properties. NP coverage and attachment on electrodes prepared through solution deposition methods can also be sensitive to surface pretreatment steps and/or NP desorption may occur over time.[6]

To preserve the core size of preformed nanoparticles during deposition, a stabilizing ligand shell is required, typically composed of electrically insulating ligands. This can pose a barrier to electron transfer throughout the NP-functionalized electrode if efforts are not made to provide an electron-tunneling pathway. Two common ways to enhance electron transfer are to form bonds between the ligands and electrode surface or other NPs in the film, or to remove the ligands through thermal or chemical treatments. Such treatments can result in growth or destabilization of the NP core.[35−37]

A strategy to improve the NP-electrode interface while retaining NP morphology is to attach NPs to an electrode via a molecular monolayer, as shown in Scheme 1. These approaches provide a molecular interface between the NP and the electrode material and allow for more control over interactions between NPs while retaining the core size control offered by use of preformed NPs. It has been shown that electron transfer from a redox probe to an electrode through a NP-molecular monolayer-electrode assembly only occurs if the NP is bound to the monolayer through electrostatic or covalent interactions.[38] Proximity to the surface alone does not seem sufficient to promote NP-mediated electron transfer. Two covalent attachment strategies are shown in Scheme 1. In the first, the NP ligand shell is used to graft the NP directly to the electrode through a functional group known to interact strongly with the electrode material (denoted X in Scheme 1). In the second case, NPs can be assembled onto chemically modified electrodes through ligand exchange with a functional group known to bind to the NP surface (denoted Y in Scheme 1). Each approach results in a defined interface for efficient electron transfer and should prevent NP desorption from the electrode surface compared to NPs that are nonspecifically adsorbed.

The assembly of nanoparticles onto a molecular monolayer has been demonstrated for larger (d_{core} >10 nm) citrate-stabilized AuNPs. These AuNPs have been assembled on molecular monolayers on planar Au,[15,38−40] glassy carbon,[14,41,42] silicon,[43] and boron doped diamond.[44,45] However, the AuNP attachment chemistry can be sensitive to pH (e.g., AuNPs assembled through Au-amine bonds) and have limited electrochemical windows (e.g., thiol monolayer desorption from planar Au at cathodic potentials in alkaline conditions[46,47]). In some cases, the electrode supports are unstable in aqueous electrolytes (e.g., silicon) limiting their general use in electrochemical applications. The use of gold electrodes makes it difficult to characterize AuNPs and to distinguish the electrochemical properties of the AuNP from those of unpassivated areas of the electrode. Some methods used to functionalize other electrode supports, particularly for carbon electrodes, yield linkers of nonuniform thicknesses[14,48] or are influenced by variable microstructure,[49] leading to uncertainty about the NP-electrode interface and irreproducible electrochemical responses. The challenges in controlling the NP-electrode interface, as well as the limited stability of these systems under electrochemical conditions, mean that these platforms are not ideal for general electrochemical study of NPs, particularly small NPs that are already more challenging to characterize.

Small NPs (d_{core} < 2.5 nm) are reported to have unique electronic and catalytic properties due to their size and their number of under-coordinated surface atoms.[16,28,50] Small changes in NP size and surface chemistry in this regime can significantly affect these properties,[51] warranting the further investigation of NPs of uniform size, well-established surface chemistry, and a defined interface between the NP and the electrode. One of the few existing electrochemical studies of small NPs bound to an electrode by a molecular monolayer was reported by Hicks et al.[52] They adhered small AuNPs (d_{core} = 1.6 nm), stabilized by a mixed hexanethiolate/mercaptoundecanoic acid ligand shell, to a planar Au electrode through Zn^{2+}/carboxylate bridges. In order to further understanding of NP-mediated electron transfer and electrocatalytic properties of NPs in this small size regime, a robust, versatile platform that

DOI: 10.1021/jacs.6b07674
J. Am. Chem. Soc. 2016, 138, 13975−13984

allows for small, uniform NPs to be attached to an electrode through molecular monolayers is needed.

Herein, two approaches to interface small AuNPs (d_{core} < 2.5 nm) to boron doped diamond (BDD) electrodes through molecular linkers have been developed and the electrochemical properties of the assemblies compared. Boron doped diamond was selected as the electrode material because it is relatively inert, has a wide electrochemical window and can be used to generate defined NP-electrode interfaces through photochemical grafting of alkenes to its surface.[53] In one approach, AuNPs are directly grafted to the electrode surface using the NP ligand shell as the covalently bound molecular linker. A second approach involves ligand exchange to link AuNPs to a molecular monolayer covalently bound to the electrode surface. The efficiency of the NP attachment chemistry was studied, showing that both methods yield monolayer coverage and that NP core size is not affected during the grafting and assembly processes. AuNPs with different core sizes and ligand shells were successfully assembled demonstrating the versatility of the platform. Using a redox probe tethered to the NP surface, the electrochemical properties of the different molecularly tethered AuNP systems were compared to one another and to those prepared by drop-casting AuNP films and depositing a AuNP monolayer formed at the air−water interface.

EXPERIMENTAL SECTION

Materials and Characterization. Water (18.2 MΩ·cm) was obtained from a Barnstead Nanopure Diamond system. Chloroform was filtered through basic alumina before use with nanoparticles to remove any acidic impurities. All other reagents were used as received without further purification. Hydrogen tetrachloroaurate was obtained from Strem Chemicals. S-(10-undecenyl)-1-thioacetate was received from Sigma-Aldrich. Electrochemical grade free-standing boron doped diamond (BDD) substrates (Element Six, 1 cm × 1 cm) were used for all experiments.

Nuclear magnetic resonance spectroscopy (^{1}H NMR) spectra were collected on a Varian Inova 300 MHz NMR to verify material purity. Ultraviolet−visible spectroscopy (UV−vis) spectra were collected using an Ocean Optics USB2000 spectrometer and samples were measured in a quartz cuvette (1 cm path length). Small angle X-ray scattering (SAXS) patterns were collected on an Anton Paar SAXSess mc^2 instrument operating in line collimation mode. The samples were measured in an epoxy sealed quartz capillary (Charles Supper) and were exposed to a monochromated X-ray source (Cu Kα, 1.54 Å) operating at 40 kV and 50 mA. Data were collected by averaging 50 scans of 5−20 s exposures. Scattered X-ray intensity was measured with a charge-coupled device (CCD) detector (Roper Scientific). Data were desmeared using the Anton Paar SAXSquant software to produce scattering patterns and were imported into the Irena macro within IGOR Pro for modeling.[54] Models were fit to the scattering patterns using a Gaussian distribution, spherical form factor, and a dilute structure factor to determine the core size distribution of the AuNPs. All reported size distributions came from the Modeling II macro within Irena. Transmission electron microscopy (TEM) images were acquired on a FEI Titan 80−300 TEM. Samples were prepared by drop-casting a dilute solution of the nanoparticles on a lacey carbon coated copper TEM grid (Ted Pella).

X-ray photoelectron spectroscopy (XPS) was performed on a ThermoScientific ESCALAB 250 X-ray Photoelectron Spectrometer using an Al Kα monochromated source (150 W, 20 eV pass energy, 500 μm spot size). The spectra were analyzed using a Smart background and were calibrated to the C 1s hydrocarbon peak (284.8 eV). Peak fitting was done using ThermoScientific Avantage 4.75 software. Scanning electron microscopy (SEM) images were collected on a Zeiss Ultra-55 Scanning Electron Microscope using a secondary electron detector at an accelerating voltage of 25 kV.

Cyclic voltammograms were collected using a BAS 100B Electrochemical Analyzer (Bioanalytical Systems). AglAgCl (3 M NaCl) reference electrodes and a platinum wire auxiliary electrode (Bioanalytical Systems) were used for all measurements. The geometric surface area of the working electrode was defined using a Viton O-ring (0.6 cm inner diameter) in a custom glass electrochemical cell. Electrical contact to the BDD electrodes was made through a back contact with silver paint and copper wire.

Synthesis and Characterization of Gold Nanoparticles. Undecenethiolate-stabilized gold nanoparticles (UDT-AuNPs) were synthesized following a modified two-phase Brust preparation.[55] $Au_{101}(PPh_3)_{21}Cl_5$ (TPP-Au_{101}) and $Au_{11}(PPh_3)_8Cl_3$ (TPP-Au_{11}) were synthesized using previously reported methods.[51,56] Nanoparticles were characterized using ^{1}H NMR, UV−vis spectroscopy, SAXS, and TEM.

Direct Functionalization of Boron Doped Diamond with UDT-AuNPs. Boron doped diamond (BDD) substrates were cleaned with aqua regia and piranha solution before hydrogen termination. Hydrogen termination, which was necessary for photochemical grafting, was performed in a tube furnace with flowing H_2 in a quartz tube under conditions reported to produce hydrogen terminated diamond surfaces.[57] The BDD was heated to 850 °C and held at that temperature for 20 min before cooling back down to room temperature under H_2. Contact angle goniometry was used to verify that the thermal treatment effectively hydrogen terminated the BDD surface. The contact angle increased from 40° to 70° after hydrogen termination, indicating an increased hydrophobicity of the BDD. The sharpening of the peak at 284.8 eV in the X-ray photoelectron spectroscopy (XPS) C 1s spectrum, attributed to C−H bonds, and the disappearance of the oxidized carbon shoulder at ∼288.6 eV indicated that the BDD was successfully hydrogen terminated (Figure S1).

The procedure for photochemical grafting was adapted from Hamers and co-workers.[53,58] To graft the UDT-AuNPs to BDD (**Graft-UDT-AuNP**), a solution of UDT-AuNPs in heptane was sparged with argon to remove oxygen. The concentration of the nanoparticle solution, measured using the absorbance of the solution at 500 nm, was ∼0.2 absorbance units. A hydrogen terminated BDD substrate was submerged in ∼1 mL of the nanoparticle solution in a 10 mL beaker and irradiated through a quartz window with a UVP UVGL-58 Hand-held UV lamp (254 nm, ∼1 mW/cm^2) for 7 h in an argon filled chamber. Photochemical grafting was performed in an argon filled chamber to minimize ozone generation during irradiation. The substrate was rinsed extensively with dichloromethane and hexanes to yield the UDT-AuNP-functionalized BDD substrate (**Graft-UDT-AuNP**).

Assembly of Triphenylphosphine Gold Nanoparticles onto Undecyl Thioacetate Modified BDD (UDTA-BDD). *Functionalization of Boron Doped Diamond Using S-10-(undecenyl) thioacetate.* An undecyl thioacetate monolayer was formed on BDD by photochemically grafting S-10-(undecenyl) thioacetate to BDD using a procedure adapted from Hamers and co-workers.[53,58] Neat S-10-(undecenyl) thioacetate (∼2 μL) was placed on a hydrogen terminated BDD substrate and sandwiched between a quartz slide to produce a film on the BDD substrate. This sample was irradiated at 254 nm for 5 h under argon in a Novascan PSD Pro Series Digital UV Ozone System. The substrate was removed and sonicated in 30 mL chloroform (2× 5 min) followed by sonication in toluene (2× 5 min) to remove any physiadsorbed thioacetate to yield **UDTA-BDD**.

Assembly of TPP-Au_{101} on UDTA-BDD (TPP-Au_{101}-UDT). **UDTA-BDD** was submerged in a solution of TPP-Au_{101} in tetrahydrofuran (0.1 mg/mL). The solution was sparged with N_2 and kept under N_2 overnight to assemble the nanoparticles on the monolayer through ligand exchange. The sample was removed and vigorously shaken in dichloromethane for 1 min (3×) to remove physiadsorbed TPP-Au_{101} and $AuClPPh_3$ from the ligand exchange.

*Assembly of TPP-Au_{11} on Undecanethiol-Functionalized BDD (**TPP-Au_{11}-UDT**).* Before assembly of TPP-Au_{11}, the thioacetate group on **UDTA-BDD** was deprotected to yield a thiol-functionalized surface. A mixture of K_2CO_3 (0.3 g, 2.2 mmol) in N_2-sparged methanol (20 mL) was stirred for 10 min. **UDTA-BDD** was

DOI: 10.1021/jacs.6b07674
J. Am. Chem. Soc. 2016, 138, 13975−13984

Scheme 2. Two Strategies to Prepare AuNP-Functionalized Electrodes with a Molecular Nanoparticle−Electrode Interface

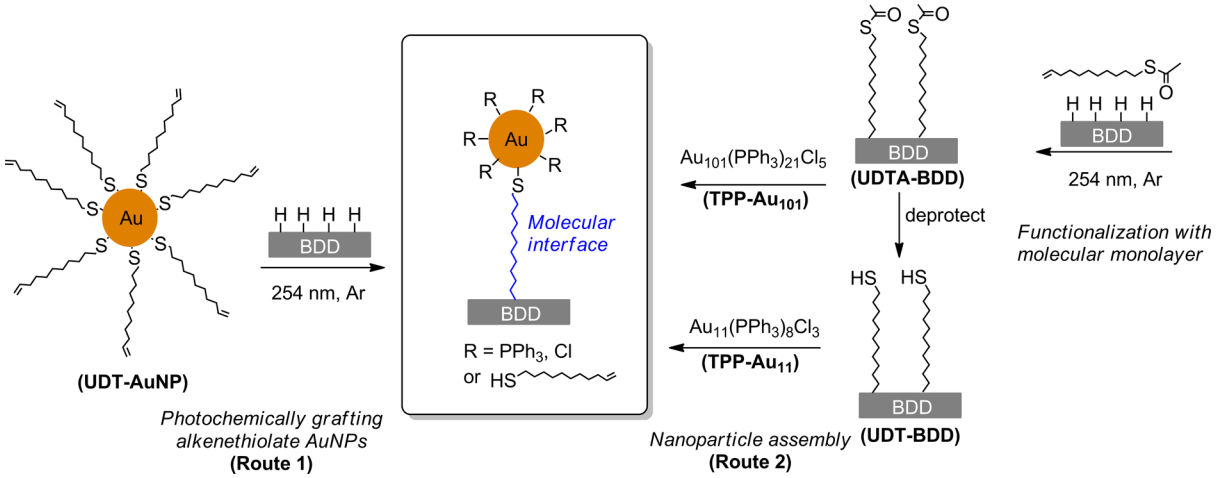

submerged in the mixture for 2 h and kept under N_2 to prevent disulfide formation. HCl (10 mL, 0.2 M, N_2 sparged) was then added to the mixture to yield the deprotected undecanethiol-functionalized BDD (**UDT-BDD**). **UDT-BDD** was removed and rinsed with dichloromethane. **UDT-BDD** was then submerged in a solution of N_2-sparged TPP-Au_{11} in basic chloroform (0.1 mg/mL). The solution was heated to 55 °C under N_2 and left to react overnight, conditions that have previously been used for ligand exchange of TPP-Au_{11}.[59] The sample was removed and vigorously rinsed in dichloromethane for 1 min (3×) to remove physiadsorbed TPP-Au_{11} and free triphenylphosphine ligand from the ligand exchange.

Binding the Redox Probe 6-Ferrocenyl(carbonyloxy)-hexanethiol ($FcCO_2HT$) to the AuNP Surface. The redox probe 6-ferrocenyl(carbonyloxy)hexanethiol ($FcCO_2HT$) was synthesized based on a method previously reported (details in the Supporting Information).[60] The **Graft-UDT-AuNP** electrodes were treated with ozone (50 ppm in N_2) for 5 min, followed by a 10 min soak in H_2O. This treatment is known to remove a portion of the thiolate ligand shell.[61] The sample was soaked in 1 mM $FcCO_2HT$ (in dichloromethane) to assemble the redox probe on the open sites on the NP, followed by extensive rinses with dichloromethane and acetonitrile to remove nonspecifically bound $FcCO_2HT$ from the surface. The **TPP-Au_x-UDT** samples were soaked in 1 mM $FcCO_2HT$ (in dichloromethane) to exchange some of the triphenylphosphine ligands for $FcCO_2HT$, followed by extensive rinses with dichloromethane to remove any unbound $FcCO_2HT$.

Deposition of Monolayer Films of AuNPs Formed by Self-Assembly at the Air−Water Interface onto BDD. A 10 mL beaker was filled with H_2O and the water surface was coated with a solution of NPs dispersed in dichloromethane. Once the dichloromethane had evaporated, the resulting monolayer of NPs was transferred to a bare BDD electrode by placing the BDD substrate on top of the NP monolayer at the air−water interface.

RESULTS AND DISCUSSION

The aim of this study was to evaluate the electrochemical properties of small, uniform ligand-stabilized AuNPs at a molecularly defined electrode interface and to evaluate the role of the interface and core size on those properties. A NP-functionalized electrode possessing a monolayer of evenly distributed NPs bound through a well-defined interface that also retain their initial core size once assembled on the surface was required for this study. Boron doped diamond (BDD) was chosen as an electrode support because it is a robust material that is electrically conductive, stable in most common electrolytes, relatively inert toward most electrocatalytic transformations, and has a wide electrochemical window.[62] Furthermore, molecular monolayers can be generated through the photochemical grafting of alkenes to form covalent C−C bonds between the BDD and the grafted molecule.[53,58] Small ligand-stabilized AuNPs (d_{core} < 2.5 nm) were chosen as a model system to assemble due to their interesting electronic and catalytic properties and since well-established synthetic methods that afford both a narrow core size distribution and defined surface chemistry exist.

Scheme 2 outlines two routes used to obtain AuNPs bound through an undecanethiolate tether to a hydrogen terminated BDD substrate. In Route 1, preformed undecenethiolate AuNPs (UDT-AuNPs) are covalently attached to the BDD through direct photochemical grafting of their ligand shell to the substrate (**Graft-UDT-AuNP**). This is a direct, single-step approach to attach synthetically accessible and stable alkene-modified AuNPs. In Route 2, two different core sizes of preformed triphenylphosphine-stabilized AuNPs (d_{core} = 0.8 and 1.9 nm) are assembled via ligand exchange onto an undecyl thioacetate-functionalized molecular monolayer covalently bound to BDD (**UDTA-BDD**). The thioacetate protecting group prevents disulfide formation and other undesired thiol-alkene reactions during the initial photochemical grafting of the linker to the substrate. The thioacetate group is easily deprotected to the free thiol prior to AuNP assembly, if needed. Triphenylphosphine-stabilzed AuNPs were used since they are known to readily undergo ligand exchange reactions with thiols.[59,63,64] An undecyl thioacetate monolayer was used to maintain a constant linker length across all three systems studied, allowing for direct comparisons to be made. The assembly approach provides a method when shorter molecular linkers are desired, and/or when NPs of a desired core material/size cannot be synthesized with terminal alkenes in their ligand shell.

Synthesis and Characterization of Ligand-Stabilized AuNPs for Attachment. Undecenethiolate-stabilized AuNPs (UDT-AuNPs) were synthesized as previously reported and purified by sequential precipitations.[55] ^{1}H NMR verified that purification removed any free ligand or phase transfer catalyst (Figure S2). The UDT-AuNPs were found to be 2.1 ± 0.1 nm by small-angle X-ray scattering (SAXS) and transmission electron microscopy (TEM) (Figure S3). The absence of a plasmon peak in the UV−vis spectrum is consistent with this size (Figure S4).

DOI: 10.1021/jacs.6b07674
J. Am. Chem. Soc. 2016, 138, 13975−13984

Two types of triphenylphosphine-stabilized AuNPs (TPP-Au_x) were synthesized for use in ligand exchange reactions with the molecular monolayer. $Au_{101}(PPh_3)_{21}Cl_5$ (TPP-Au_{101}) was synthesized as previously reported.[56] The core size of TPP-Au_{101} was determined to be 1.9 ± 0.5 nm by SAXS, and was corroborated by TEM and UV−vis (Figure S5, S6). $Au_{11}(PPh_3)_8Cl_3$ (TPP-Au_{11}) was synthesized by reduction of $AuClPPh_3$ with $NaBH_4$.[51] ^1H NMR and UV−vis of TPP-Au_{11} confirmed that only $Au_{11}(PPh_3)_8Cl_3$ was synthesized and not a mixture of $Au_{11}(PPh_3)_8Cl_3$ and the less stable form $Au_{11}(PPh_3)_7Cl_3$ (Figure S7, S8).[51] The core size of TPP-Au_{11} was determined to be 0.8 ± 0.2 nm by TEM (N = 530) (Figure S8).

Building the AuNP-Molecular Monolayer-BDD Platform. *Route 1: Photochemically Grafting Undecenethiolate AuNPs to BDD (**Graft-UDT-AuNP**).* UDT-AuNPs were grafted to BDD upon irradiation of BDD in a dilute heptane solution of UDT-AuNPs at 254 nm under argon. X-ray photoelectron spectroscopy (XPS) of **Graft-UDT-AuNP** was performed to determine if the UDT-AuNPs were altered by the grafting process (Figure S9). The elemental $Au_{84.5}$:$S_{162.5}$ ratio was used to compare the thiolate ligand shell before and after the grafting process, since 162.5 eV is the characteristic binding energy of a thiol. There was minimal change in the $Au_{84.5}$:$S_{162.5}$ ratio when the UDT-AuNPs are grafted versus when they were simply drop-cast onto a BDD substrate (Table 1) indicating the integrity of the ligand shell of the UDT-AuNPs is maintained throughout the grafting process. The difference in $Au_{84.5}$:$S_{162.5}$ ratios between the two samples can be explained by ozone generated in the grafting chamber from trace oxygen resulting in the oxidation of a small amount of the thiolate ligands in the **Graft-UDT-AuNP** sample.

Table 1. Comparison of Elemental Ratios of UDT-AuNPs on BDD by XPS

sample	$Au_{84.5}$:$S_{162.5}$	$Au_{84.5}$:$C_{284.8}$
Drop-cast sample[a]	2.9 ± 0.1[b]	–
Graft-UDT-AuNP	3.4 ± 0.2[b]	0.12 ± 0.02[b]
Control sample, no UV[c]	3.3 ± 0.1[d]	0.020 ± 0.002[d]

[a]Sample prepared by drop-casting UDT-AuNPs onto BDD substrate. [b]Average of two samples, three spots analyzed per sample. [c]Sample exposed to all grafting conditions except irradiation by 254 nm light. [d]Average of three spots on one sample.

A control experiment was performed to assess if the XPS Au 4f signal was due to grafting UDT-AuNPs or simply AuNP physiadsorption to the BDD surface. A bare BDD substrate was treated in the same way as the **Graft-UDT-AuNP** samples except that it was not irradiated by 254 nm light. The $Au_{84.5}$:$C_{284.8}$ ratio obtained via XPS was used to compare AuNP surface coverage over the BDD substrate. The $Au_{84.5}$:$C_{284.8}$ ratio underestimates the true coverage since the C 1s peak at 284.8 eV originates from both the BDD substrate as well as the alkenethiolate ligand shell. The **Graft-UDT-AuNP** sample has roughly an order of magnitude higher $Au_{84.5}$:$C_{284.8}$ ratio compared to the sample that was not irradiated (Table 1). This suggests that the majority of the Au 4f XPS signal is not a result of physiadsorbed AuNPs, and that the UDT-AuNPs were successfully grafted to BDD.

Route 2: TPP-Au_x NP Assembly onto Undecanethiolate Monolayers on BDD. Before AuNP assembly, an undecyl thioacetate molecular monolayer was grafted to BDD by irradiation at 254 nm under argon to produce **UDTA-BDD** as shown in Scheme 2. XPS was used to evaluate the efficacy of the photochemical grafting method in forming an undecyl thioacetate monolayer on BDD. The S 2p region of the XPS of **UDTA-BDD** showed a peak at 164.2 eV, characteristic of a thioacetate group (Figure S10). A control experiment was performed where a hydrogen terminated BDD (H-BDD) substrate was exposed to 10-undecene-1-thioacetate in the dark. The grafted **UDTA-BDD** and the control sample were compared with XPS using the $S_{164.2}$:$C_{284.8}$ elemental ratios as a metric to evaluate the extent of thioacetate grafting. The grafted thioacetate yielded a $S_{164.2}$:$C_{284.8}$ ratio of 0.023 ± 0.007 (determined from averaging four samples), while the control sample only had a $S_{164.2}$:$C_{284.8}$ ratio of 0.002. This verifies the efficacy of the photochemical grafting and confirms that the

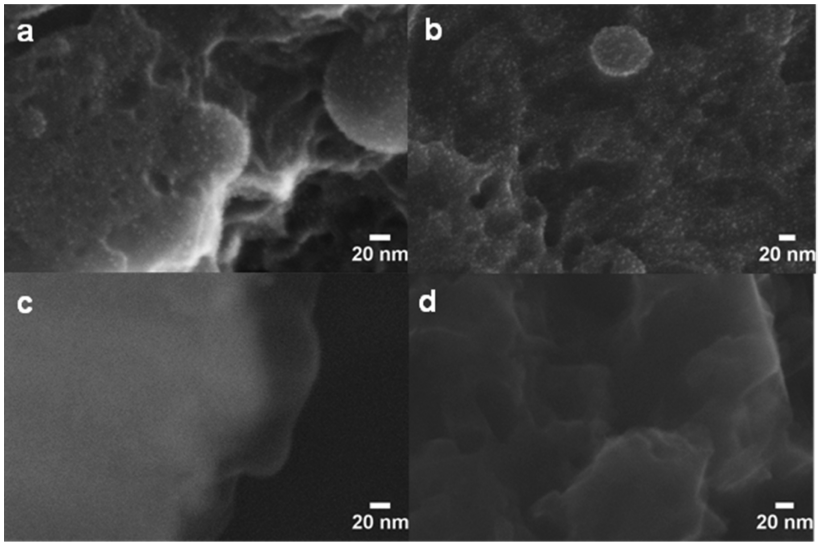

Figure 1. SEM images of (a) **Graft-UDT-AuNP**, (b) **TPP-Au_{101}-UDT**, (c) a bare BDD substrate, and (d) **UDTA-BDD**. The small, white features in (a) and (b) demonstrate the methods yield monolayer coverage of nanoparticles, and the absence of these features in (c) and (d) verify that these features are indeed nanoparticles and do not originate from the substrate.

DOI: 10.1021/jacs.6b07674
J. Am. Chem. Soc. 2016, 138, 13975−13984

thioacetate signal observed in **UDTA-BDD** is due primarily to grafting, not physiadsorption to the BDD surface. Cyclic voltammetry was used to assess the extent of BDD passivation. The **UDTA-BDD** electrode showed an 87% decrease in capacitive current and significant suppression of oxygen reduction current compared to the H-BDD electrode (Figure S11).

Ligand exchange reactions were used to tether TPP-Au_{101} to **UDTA-BDD**. The $Au_{84.5}$:$C_{284.8}$ elemental ratios from XPS were used to compare AuNP surface coverage between samples. When **UDTA-BDD** was exposed to TPP-Au_{101}, XPS yielded a $Au_{84.5}$:$C_{284.8}$ ratio of 0.15 ± 0.07 whereas a bare BDD substrate exposed to TPP-Au_{101} yielded a $Au_{84.5}$:$C_{284.8}$ ratio of 0.05 ± 0.01. In addition, XPS provided evidence that TPP-Au_{101} is assembled on **UDTA-BDD** through Au-thiolate bonds from the appearance of a new peak in the S 2p spectrum at a lower binding energy, ∼162.8 eV, indicative of a Au-thiolate bond (Figure S12). In addition to the presence of the thiolate bond, a P 2p peak at 131.2 eV and Cl 2p peak at 197.8 eV are also present, indicating that the portion of the TPP-Au_{101} ligand shell that does not undergo ligand exchange remains intact throughout the assembly process (Figure S12).

TPP-Au_{11} could also be assembled on BDD through undecanethiolate linkers, but first required deprotection of the terminal thioacetate in **UDTA-BDD** to yield a surface rich in thiol groups (**UDT-BDD**). When **UDT-BDD** was exposed to TPP-Au_{11}, XPS yielded a $Au_{84.5}$:$C_{284.8}$ ratio of 0.10 ± 0.06 while a bare BDD substrate exposed to TPP-Au_{11} yielded a $Au_{84.5}$:$C_{284.8}$ ratio of 0.005 ± 0.001. The characteristic peak for a Au-thiolate bond also appeared in the XPS S 2p spectrum which suggests that TPP-Au_{11} is bound to the molecular monolayer surface through Au-thiolate bonds (Figure S13). The ability of the system to assemble both TPP-Au_{101} and TPP-Au_{11} exemplifies its versatility.

Assessing Surface Coverage of AuNPs on BDD. While $Au_{84.5}$:$C_{284.8}$ ratios from XPS provided a means of comparing the Au surface coverage between samples, a method was needed to determine NP surface coverage more directly. Figure 1a,b shows scanning electron microscope (SEM) images of **Graft-UDT-AuNP** and **TPP-Au_{101}-UDT** samples showing even AuNP coverage with no signs of NP aggregation. In comparison, the bare BDD and **UDTA-BDD** show no features in this size range at the same magnification (Figure 1c,d). Due to the small size of the AuNPs, the SEM is near its resolution limit, preventing quantitative size analysis of the AuNPs; however, it is still possible to estimate the coverage of nanoparticles from these images. The coverage of AuNPs obtained via molecular tethering is estimated to be ∼10^{11} NPs/cm^2 for both the **Graft-UDT-AuNP** and **TPP-Au_{101}-UDT** samples, determined by counting NPs on the SEM images. Using the NP core diameter and ligand shell contribution to determine the NP area, and assuming the NPs are monodisperse and the BDD is flat, the theoretical coverage of a hexagonally close packed monolayer was calculated. The tethered samples yield approximately 10% NP coverage relative to a theoretical monolayer of NPs. For comparison, other methods reported to assemble monolayers of ∼13 nm citrate-stabilized AuNPs on planar supports through molecular tethers resulted in ∼1−30% coverage of AuNPs relative to a theoretical monolayer of NPs.[38,44,45]

Assessing Nanoparticle-Mediated Electron Transfer Using a AuNP Tethered Redox Probe. A small amount of a redox probe, 6-ferrocenyl(carbonyloxy)hexanethiol ($FcCO_2HT$), was introduced into the ligand shell of the AuNPs through Au-thiolate bonds to electrochemically evaluate the AuNP-UDT systems. A redox probe bound to the NP surface was chosen to examine NP-mediated electron transfer instead of a redox probe in solution to minimize any direct electron transfer between the redox probe and the BDD electrode support. $FcCO_2HT$ was chosen because of its fast electron transfer, allowing for the electron transfer from the NP to the electrode to be directly observed.[40] In addition, the hydrophilic ester moiety prevents the ferrocene from burying itself in the hydrophobic alkane monolayer. This probe also facilitates the comparison of this platform to existing reports of planar Au self-assembled monolayers of ferrocene thiols.[60]

Two different methods were used to attach $FcCO_2HT$ to the AuNP surface for the **Graft-UDT-AuNP** samples and the **TPP-Au_x-UDT** samples. The **Graft-UDT-AuNP** sample was initially treated with dilute ozone to remove a portion of the thiolate ligand shell. The $FcCO_2HT$ probe was then introduced to replace the partially removed thiolate ligand shell. This method was used in lieu of a direct ligand exchange between the $FcCO_2HT$ and the undecenethiolate ligands because thiol for thiol ligand exchanges do not always readily occur, especially when trying to replace a longer chain ligand with a shorter ligand.[65] This dilute ozone treatment was previously shown not to cause NP growth or destabilization.[61] $FcCO_2HT$ was attached to **TPP-Au_x-UDT** samples through simple ligand exchange with the triphenylphosphine ligands.[59,63] Chart 1 depicts the two molecularly tethered AuNP systems with bound $FcCO_2HT$ redox probes.

Chart 1. Molecularly Tethered AuNP-Functionalized Boron Doped Diamond Electrodes with Bound Ferrocene (Fc) Redox Probes

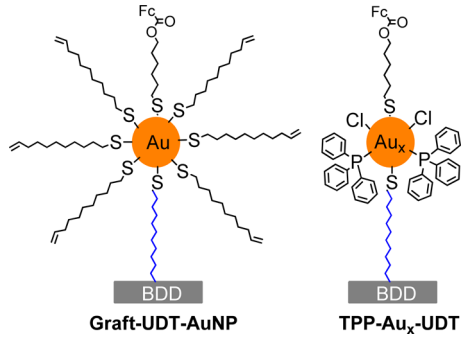

Several control experiments were performed to ensure the measured current was from redox probe bound to the NP surface. To ensure the $FcCO_2HT$ signal was only from ferrocenes bound to the AuNPs (rather than directly to the BDD), a bare substrate was treated in the same manner used to attach $FcCO_2HT$ to the **Graft-UDT-AuNP** samples (Figure S14). No $FcCO_2HT$ signal was detected, indicating that $FcCO_2HT$ does not attach directly to the BDD surface. It was also possible in the **TPP-Au_x-UDT** systems that the $FcCO_2HT$ could form disulfide bonds with free terminal thioacetate or thiol functionalities in the molecular monolayer. To investigate this scenario, **UDTA-BDD**, **TPP-Au_{101}-UDT**, and **TPP-Au_{11}-UDT** were treated with known disulfide reducing agents (dithiothreitol or tris(2-carboxyethyl)phosphine (TCEP)) to reduce any disulfide bonds between the molecular monolayer and the redox probe (Figures S15, S16). A small reduction in faradaic current was observed, however, the peak potentials

DOI: 10.1021/jacs.6b07674
J. Am. Chem. Soc. 2016, 138, 13975−13984

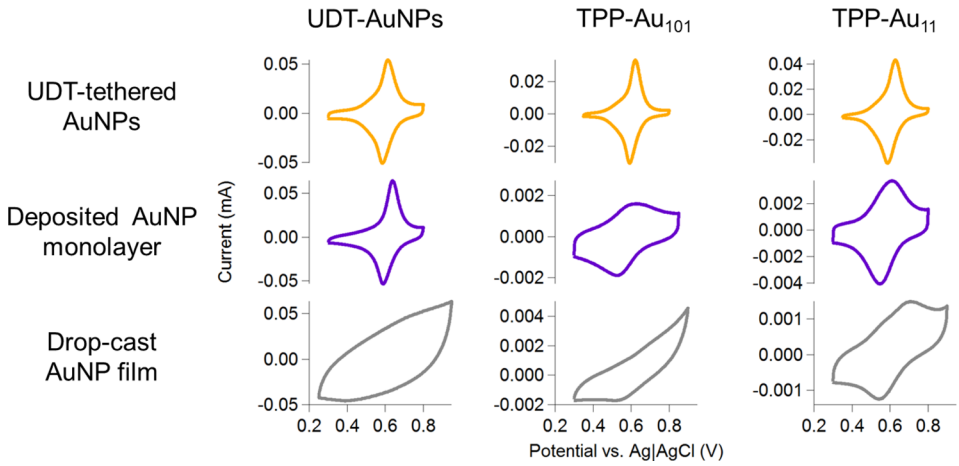

Figure 2. Comparison of cyclic voltammograms of the AuNP-BDD electrodes fabricated by different methods: binding a monolayer of AuNPs through an undecanethiolate monolayer (top row), depositing a AuNP monolayer film formed by self-assembly at the air−water interface (middle row), and drop-casting a AuNP film (bottom row). All samples were treated with $FcCO_2HT$. CVs were taken in 0.1 M $HClO_4$ at 100 mV/s.

Table 2. Electrochemical Properties of the $FcCO_2HT$-AuNP-BDD Electrodes

AuNP sample	NP-attachment method	ΔE_p (mV)	fwhm (anodic) (mV)	$E^{0\prime}$ (mV)	electrochemically active Au surface area (cm^2)
UDT-AuNP	UDT-tethered	30	90	601	0.9 ± 0.3[c]
	Deposited monolayer	50	78	615	0.9
	Drop-cast	N/A[a]	N/A[a]	N/A[a]	1.2
$TPP\text{-}Au_{101}$	UDT-tethered	28	68	607	0.43 ± 0.03[c]
	Deposited monolayer	101	>400	580	0.02
	Drop-cast	N/A[a]	N/A[a]	N/A[a]	N/A[b]
$TPP\text{-}Au_{11}$	UDT-tethered	41	84	609	0.5 ± 0.3[c]
	Deposited monolayer	65	170	580	0.01
	Drop-cast	168	>300	627	0.02

[a]Unable to identify clear $FcCO_2HT$ signal. [b]Characteristic sharp Au oxide reduction peak not present. [c]Averaged over three samples.

remained unchanged. Finally, to further confirm that the observed current only originated from probe bound to the NP, **Graft-UDT-AuNP** was treated with a 0.1 M KCN solution to decompose the AuNPs. Less than 10% of the initial $FcCO_2HT$ remained in the cyclic voltammograms of the decomposed sample, suggesting that the majority of the current in the original **Graft-UDT-AuNP** sample is from NP-bound redox probe (Figure S17).

Effect of Molecular Tethering Method and NP Core Size on Electrochemical Properties. Cyclic voltammetry (CV) was used to investigate the electrochemical properties of the $FcCO_2HT$-AuNP-UDT systems (Figure 2, top row). All three systems exhibit behavior of a reversible, surface bound redox probe where the peak current scales linearly with the scan rate (Figure S18), and are stable over many electrochemical cycles. Slightly different peak-to-peak separations (ΔE_p), full width at half-maximum (fwhm), and $E^{0\prime}$ values were found for each system (Table 2). ΔE_p can be used to assess the barrier to electron transfer. For an ideal surface bound redox probe, the ΔE_p is 0 mV. The small $\Delta E_p \leq 41$ mV for all three $FcCO_2HT$-AuNP-UDT systems indicates the undecanethiolate molecular tether does not significantly inhibit electron transfer. The **Graft-UDT-AuNP** (d_{core} = 2.1 ± 0.1 nm) and the **$TPP\text{-}Au_{101}$-UDT** (d_{core} = 1.9 ± 0.5 nm) systems had ΔE_p values within 2 mV of each other, 30 mV and 28 mV respectively, while the smaller **$TPP\text{-}Au_{11}$-UDT** (d_{core} = 0.8 ± 0.2 nm) system had a ΔE_p of 41 mV. The larger ΔE_p suggests the **$TPP\text{-}Au_{11}$-UDT** system experiences a greater barrier to electron transfer than the **Graft-UDT-AuNP** and **$TPP\text{-}Au_{101}$-UDT** samples. Chazalviel and Allongue theorized that the rate of NP-mediated electron transfer across a molecular monolayer is dependent on both molecular layer thickness and NP core size, with electron transfer being more hindered as NP size is decreased.[66] The similar ΔE_p values for the similarly sized AuNP systems and larger ΔE_p exhibited by the smaller, **$TPP\text{-}Au_{11}$-UDT** system is in agreement with Chazalviel's theoretical model. The fwhm for all three systems are near 90 mV, the ideal value for a surface bound redox couple. This suggests there are no major ferrocene-ferrocene interactions in the $FcCO_2HT$-AuNP-UDT systems as such interactions would broaden both the anodic and cathodic peaks. The narrow fwhm values also suggest that spatial inhomogeneity in electron transfer rates reported for BDD[67,68] do not significantly influence the results reported here. Lastly, both **$TPP\text{-}Au_x$-UDT** samples' $E^{0\prime}$ values were within 2 mV of each other while the **Graft-UDT-AuNP** system's $E^{0\prime}$ value was decreased by 6−8 mV. This could suggest that $E^{0\prime}$ is ligand shell dependent and not dependent on core size. The variance in electrochemical properties with changing NP size is evidence that the observed electron transfer is NP-mediated. Both molecular tethering routes yield almost identical electrochemical properties, where $E^{0\prime}$ is slightly affected by the ligand shell. Either route is suitable to fabricate a NP-functionalized electrode with a uniform monolayer of

DOI: 10.1021/jacs.6b07674
J. Am. Chem. Soc. 2016, 138, 13975−13984

molecularly tethered NPs that exhibits reproducible electrochemical behavior.

Although it is tempting to compare the $FcCO_2HT$-AuNP-UDT systems to analogous AuNP-SAM-electrode systems, most AuNP-SAM-electrode systems employ passivating monolayers and thus are able to use solution phase redox probes for electrochemical characterization. Since the molecular monolayers formed on boron doped diamond are not completely passivating,[69] the electrochemical response observed from a solution redox probe in the AuNP-UDT-BDD system arises from both AuNPs and the BDD substrate. Liu et al. reported a AuNP-SAM-electrode system studied with a tethered redox probe assembled AuNPs (d_{core} = 5−15 nm) on terminal thiol SAMs.[40] However, they used a very fast scan rate, 50 V/s, preventing the comparison of ΔE_p values due to its scan rate dependence, sample preparation and peak shapes can be compared. The 6-(ferrocenyl) hexanethiol probe they used was diluted 1:9 with 1-pentanethiol to prevent major ferrocene-ferrocene interactions. Even with their use of a diluent ligand, the CV has a prominent anodic shoulder indicating the ferrocene probe resides in different local environments. Similarly, Kondo et al. reported assembly of large AuNPs (∼12 nm) on 3-mercaptopropyltrimethoxysilane linkers on boron doped diamond, also using bound 6-(ferrocenyl) hexanethiol to electrochemically evaluate their samples.[45] While they ran CVs in 0.1 M $NaHCO_3$, preventing direct comparison of $E^{0\prime}$ values, the fwhm values of their system were almost double compared to the $FcCO_2HT$-AuNP-UDT samples reported in this work. They also observed small ΔE_p values (∼17 mV). The slightly smaller ΔE_p values in their system are likely a result of the larger AuNP core size and that their molecular linker is a third of the length of the undecanethiolate linkers used in this work, both of which have been reported to influence electron transfer.[38,66] The $FcCO_2HT$-AuNP-UDT systems do not require the use of a diluent ligand to achieve narrow redox peaks. This could be due to the uniform spacing of AuNPs across the BDD, allowing for each $FcCO_2HT$ molecule to reside in chemically equivalent environments.

Effect of NP Attachment Method on Electrochemical Properties: Molecular Tethering, Deposition of a Monolayer, and Drop-Casting. NPs tethered to electrodes through a molecular interface were compared to electrodes prepared by other solution deposition techniques. One simple method often used to prepare NP monolayers (or submonolayers) on electrodes is NP self-assembly at the air−water interface, followed by transfer of the NP monolayer to the electrode.[70−72] A AuNP monolayer was formed through self-assembly at an air−water interface and then deposited on a BDD electrode. This sample was then treated with $FcCO_2HT$ to directly compare the effect of the molecular interface on the electrochemical properties (Figure 2, middle row). All three samples prepared through deposition of a AuNP monolayer to BDD had larger ΔE_p values than their respective UDT-tethered samples (Table 2). These larger values suggest that the barrier to electron transfer increases in the absence of a covalent molecular interface. For the TPP-Au_x samples, the fwhms were significantly broader than their tethered analogues, indicating that the environment of $FcCO_2HT$ is not uniform. The $E^{0\prime}$ for both TPP-Au_x samples prepared by deposition of the NP monolayer decreased to 580 mV while the UDT-AuNP $E^{0\prime}$ increased to 615 mV supporting the previous claim that redox potential is dependent on ligand shell. The broad redox peaks and subsequently ill-defined electrochemical properties of the physically adsorbed NP monolayer further demonstrate the necessity of strong interactions between the NP and the electrode to facilitate efficient electronic communication between the redox probe and electrode.

The electrochemical properties of molecularly tethered NPs were also compared to thicker, drop-cast NP samples. Drop-cast NP films were prepared from casting a solution of AuNPs in dichloromethane onto BDD resulting in ∼2 mg of AuNPs on the BDD electrodes. Each sample was then treated with $FcCO_2HT$ for a direct comparison. CVs of drop-cast TPP-Au_{101} and the UDT-AuNPs showed no distinct $FcCO_2HT$ redox peaks while the drop-cast TPP-Au_{11} sample showed broad $FcCO_2HT$ redox peaks with a large ΔE_p of 170 mV (Figure 2, bottom row). There were significantly more AuNPs on the drop-cast samples than the samples prepared through NP grafting or assembly, thus a much larger current response is expected if all of the NPs are available to perform electrochemistry. However, this is not observed in the CVs, presumably because only the NPs at the surface of the sample are accessible to the $FcCO_2HT$ probe and electrochemically. The ill-defined or absent $FcCO_2HT$ redox peaks for the drop-cast AuNP electrodes indicates an efficient electron transfer pathway is lacking between the redox probe and the electrode, either due to poor electrical contact between the NPs and the electrode or the physical distance between the $FcCO_2HT$-functionalized NPs and the electrode. Similar results were observed in previous work examining multilayer films of ferrocenated AuNPs.[72] These results demonstrate that one cannot simply drop-cast thicker layers of ligand-stabilized NPs onto electrode substrates as a means of increasing NP loading, for applications such as electrocatalysis, since the NP-electrode interface greatly affects the electrochemical properties.

To compare the electrochemically active surface areas of these samples, the Au surface area was determined for each sample by integration of the gold oxide reduction peak at 0.9 V vs AglAgCl in cyclic voltammograms (Figure S19).[73] For the molecularly tethered samples, the reduction peak did not disappear after multiple cycles, suggesting that the AuNPs are strongly tethered to the electrode. Additionally, the electrochemically active Au surface area of the TPP-Au_x deposited monolayer and drop-cast samples is an order of magnitude lower than their molecularly tethered analogues. This could indicate that the NPs are not as electrochemically accessible as the tethered NPs or that NP desorption occurs throughout the $FcCO_2HT$ treatment and/or electrochemical measurements. Although the differences in electrochemically active surface area between the systems are not fully understood, one possible reason a trend in surface area was not observed for the UDT-AuNP samples could be due to their exposure to ozone to remove a portion of the thiolate ligand shell prior to $FcCO_2HT$ attachment. This ozone treatment leads to more electrochemically active sites which are not produced in the TPP-Au_x systems and may also explain the differences between the electrochemically active surface areas of **Graft-UDT-AuNP** and **TPP-Au_{101}-UDT**, despite similar NP coverage.

The clear differences between the deposited monolayer and the drop-cast samples demonstrated that the electrochemical properties of NP electrodes fabricated from solution deposition techniques are variable from sample to sample. Such variability is due to a lack of control over NP-NP interactions and the NP-electrode interface. In contrast, the molecularly tethered systems exhibit reproducible electrochemical properties.

DOI: 10.1021/jacs.6b07674
J. Am. Chem. Soc. 2016, 138, 13975−13984

These results exemplify the importance of a defined interface when studying the electrochemical properties of NP-functionalized electrodes.

CONCLUSIONS

Two strategies were demonstrated for tethering small (d_{core} < 2.5 nm) ligand-stabilized AuNPs to a boron doped diamond electrode through a molecular interface. The NPs retain their composition, initial core size and shape throughout the process and yield uniform monolayer NP assemblies with ~10^{11} NPs/cm^2 coverage resulting from either method. Nanoparticle-mediated electron transfer through molecular monolayers was evaluated by attaching redox probes to the AuNP surfaces. The smaller **TPP-Au$_{11}$-UDT** system exhibits a greater barrier to electron transfer than the larger **Graft-UDT-AuNP** and **TPP-Au$_{101}$-UDT** systems as might be expected if the nanoparticle core size influences electron transfer as theorized by Chazaviel and Allongue.[66] In all cases, the molecular NP-electrode interface results in more efficient electron transfer than the two solution deposited samples, and a greater proportion of the nanoparticles are electrochemically active when using a molecular tether. In contrast to samples produced by solution deposition methods where the electrochemical response depends strongly on the exact deposition conditions, the electrochemical properties of the molecularly tethered samples were reproducible across a number of preparations.

This molecular tethering strategy offers a versatile platform to interface nanoparticles with an otherwise inert electrode material. Because the platform yields samples with reproducible electrochemical responses, it provides the opportunity to quantitatively study NP-mediated electron transfer as a function of NP morphology and linker length. It also provides a system to study the influence of core size and the NP-electrode interface on the electrocatalytic behavior of preformed nanoparticles. Both will be the focus of future work with this platform. In addition, the platform should prove useful for grafting other nanomaterials stabilized by ligands possessing terminal alkenes or assembling other nanoparticle core materials onto an appropriate terminal functional group on the monolayer. This approach could be further expanded to attach nanoparticles to substrates other than BDD where alkenes can be photochemically grafted, such as silicon, SiO_2, TiO_2, and amorphous carbon.[74−77]

ASSOCIATED CONTENT

Supporting Information

The Supporting Information is available free of charge on the ACS Publications website at DOI: 10.1021/jacs.6b07674.

Details of synthesis of 6-ferrocenyl(carbonyloxy)-hexanethiol, AuNP characterization data (^{1}H NMR, UV−vis spectra, TEM images, SAXS patterns with model fits), XPS spectra of the samples, representative cyclic voltammogram for determining electrochemically active surface area, and control experiments with KCN and disulfide reducing agents. (PDF)

AUTHOR INFORMATION

Corresponding Author

*hutch@uoregon.edu

Author Contributions

†S. L. Young and J. E. Kellon contributed equally.

Notes

The authors declare no competing financial interest.

ACKNOWLEDGMENTS

This work was supported by National Science Foundation (NSF) grant IIP-1237890. The NMR instrument facility at the University of Oregon is supported by NSF grant CHE-1427987. The authors would like to acknowledge Joshua Razink for acquisition of the TEM images and Meredith C. Sharps for acquisition of the SEM images.

REFERENCES

(1) Saha, K.; Agasti, S. S.; Kim, C.; Li, X.; Rotello, V. M. *Chem. Rev.* **2012**, *112*, 2739−2779.
(2) Segev-Bar, M.; Haick, H. *ACS Nano* **2013**, *7*, 8366−8378.
(3) Oszajca, M. F.; Bodnarchuk, M. I.; Kovalenko, M. V. *Chem. Mater.* **2014**, *26*, 5422−5432.
(4) Oezaslan, M.; Hasché, F.; Strasser, P. *J. Phys. Chem. Lett.* **2013**, *4*, 3273−3291.
(5) Corma, A.; Garcia, H. *Chem. Soc. Rev.* **2008**, *37*, 2096−2126.
(6) Kleijn, S. E. F.; Lai, S. C. S.; Koper, M. T. M.; Unwin, P. R. *Angew. Chem., Int. Ed.* **2014**, *53*, 3558−3586.
(7) Schünemann, S.; Dodekatos, G.; Tüysüz, H. *Chem. Mater.* **2015**, *27*, 7743−7750.
(8) Zhu, M.; Diao, G. *J. Phys. Chem. C* **2011**, *115*, 24743−24749.
(9) Taniguchi, K.; Jin, X.; Yamaguchi, K.; Mizuno, N. *Chem. Commun.* **2015**, *51*, 14969−15082.
(10) Willner, I.; Willner, B. *Nano Lett.* **2010**, *10*, 3805−3815.
(11) Yu, A.; Liang, Z.; Cho, J.; Caruso, F. *Nano Lett.* **2003**, *3*, 1203−1207.
(12) Tsukamoto, D.; Shiraishi, Y.; Sugano, Y.; Ichikawa, S.; Tanaka, S.; Hirai, T. *J. Am. Chem. Soc.* **2012**, *134*, 6309−6315.
(13) Tang, Y.; Cheng, W. *Langmuir* **2013**, *29*, 3125−3132.
(14) Barfidokht, A.; Ciampi, S.; Luais, E.; Darwish, N.; Gooding, J. J. *Anal. Chem.* **2013**, *85*, 1073−1080.
(15) Bradbury, C. R.; Zhao, J.; Fermín, D. J. *J. Phys. Chem. C* **2008**, *112*, 10153−10160.
(16) Kauffman, D. R.; Alfonso, D.; Matranga, C.; Qian, H.; Jin, R. *J. Am. Chem. Soc.* **2012**, *134*, 10237−10243.
(17) Cao, Z.; Kim, D.; Hong, D.; Yu, Y.; Xu, J.; Lin, S.; Wen, X.; Nichols, E. M.; Jeong, K.; Reimer, J. A.; Yang, P.; Chang, C. J. *J. Am. Chem. Soc.* **2016**, *138*, 8120−8125.
(18) Zhu, W.; Michalsky, R.; Metin, O.; Lv, H.; Guo, S.; Wright, C. J.; Sun, X.; Peterson, A. A.; Sun, S. *J. Am. Chem. Soc.* **2013**, *135*, 16833−16836.
(19) Wang, J. X.; Inada, H.; Wu, L.; Zhu, Y.; Choi, Y.; Liu, P.; Zhou, W. P.; Adzic, R. R. *J. Am. Chem. Soc.* **2009**, *131*, 17298−17302.
(20) Padayachee, D.; Golovko, V.; Ingham, B.; Marshall, A. T. *Electrochim. Acta* **2014**, *120*, 398−407.
(21) Lee, H. *RSC Adv.* **2014**, *4*, 41017−41027.
(22) Seidel, Y. E.; Schneider, A.; Jusys, Z.; Wickman, B.; Kasemo, B.; Behm, R. J. *Langmuir* **2010**, *26*, 3569−3578.
(23) Diao, P.; Guo, M.; Zhang, Q. *J. Phys. Chem. C* **2008**, *112*, 7036−7046.
(24) Sun, X.; Guo, S.; Liu, Y.; Sun, S. *Nano Lett.* **2012**, *12*, 4859−4863.
(25) Weng, Z.; Liu, W.; Yin, L. C.; Fang, R.; Li, M.; Altman, E. I.; Fan, Q.; Li, F.; Cheng, H. M.; Wang, H. *Nano Lett.* **2015**, *15*, 7704−7710.
(26) Diao, P.; Zhang, D.; Wang, J.; Zhang, Q. *Electrochem. Commun.* **2010**, *12*, 1622−1625.
(27) Tang, Y.; Cheng, W. *Nanoscale* **2015**, *7*, 16151−16164.
(28) Chen, W.; Chen, S. *Angew. Chem., Int. Ed.* **2009**, *48*, 4386−4389.
(29) Reske, R.; Mistry, H.; Behafarid, F.; Cuenya, B. R.; Strasser, P. *J. Am. Chem. Soc.* **2014**, *136*, 6978−6986.
(30) Salehi-Khojin, A.; Jhong, H. R. M.; Rosen, B. A.; Zhu, W.; Ma, S.; Kenis, P. J. A.; Masel, R. I. *J. Phys. Chem. C* **2013**, *117*, 1627−1632.

DOI: 10.1021/jacs.6b07674
J. Am. Chem. Soc. 2016, 138, 13975−13984

(31) Masuda, H.; Yasui, K.; Nishio, K. *Adv. Mater.* **2000**, *12*, 1031−1033.
(32) Penner, R. M. *J. Phys. Chem. B* **2002**, *106*, 3339−3353.
(33) Ivanova, O. S.; Zamborini, F. P. *Anal. Chem.* **2010**, *82*, 5844−5850.
(34) Lopez-Serrano, A.; Olivas, R. M.; Landaluze, J. S.; Camara, C. *Anal. Methods* **2014**, *6*, 38−56.
(35) Smith, B. L.; Hutchison, J. E. *J. Phys. Chem. C* **2013**, *117*, 25127−25137.
(36) Lopez-Sanchez, J. A.; Dimitratos, N.; Hammond, C.; Brett, G. L.; Kesavan, L.; White, S.; Miedziak, P.; Tiruvalam, R.; Jenkins, R. L.; Carley, A. F.; Knight, D.; Kiely, C. J.; Hutchings, G. J. *Nat. Chem.* **2011**, *3*, 551−556.
(37) Kilmartin, J.; Sarip, R.; Grau-Crespo, R.; Di Tommaso, D.; Hogarth, G.; Prestipino, C.; Sankar, G. *ACS Catal.* **2012**, *2*, 957−963.
(38) Shein, J. B.; Lai, L. M. H.; Eggers, P. K.; Paddon-Row, M. N.; Gooding, J. J. *Langmuir* **2009**, *25*, 11121−11128.
(39) Jensen, P. S.; Chi, Q.; Grumsen, F. B.; Abad, J. M.; Horsewell, A.; Schiffrin, D. J.; Ulstrup, J. *J. Phys. Chem. C* **2007**, *111*, 6124−6132.
(40) Liu, F.; Khan, K.; Liang, J.-H.; Yan, J.-W.; Wu, D.-Y.; Mao, B.-W.; Jensen, P. S.; Zhang, J.; Ulstrup, J. *ChemPhysChem* **2013**, *14*, 952−957.
(41) Liu, G.; Luais, E.; Gooding, J. J. *Langmuir* **2011**, *27*, 4176−4183.
(42) Matyjewicz, J.; Lesniewski, A.; Niedziolka-Jonsson, J. *Electrochem. Commun.* **2014**, *48*, 73−76.
(43) Le Saux, G.; Ciampi, S.; Gaus, K.; Gooding, J. J. *ACS Appl. Mater. Interfaces* **2009**, *1*, 2477−2483.
(44) Tian, R.; Rao, T. N.; Einaga, Y.; Zhi, J. *Chem. Mater.* **2006**, *18*, 939−945.
(45) Kondo, T.; Aoshima, S.; Honda, K.; Einaga, Y.; Fujishima, A.; Kawai, T. *J. Phys. Chem. C* **2007**, *111*, 12650−12657.
(46) Widrig, C. A.; Chung, C.; Porter, M. D. *J. Electroanal. Chem. Interfacial Electrochem.* **1991**, *310*, 335−359.
(47) Boubour, E.; Lennox, R. B. *Langmuir* **2000**, *16*, 7464−7470.
(48) Mattiuzzi, A.; Jabin, I.; Mangeney, C.; Roux, C.; Reinaud, O.; Santos, L.; Bergamini, J.-F.; Hapiot, P.; Lagrost, C. *Nat. Commun.* **2012**, *3*, 1130.
(49) McCreery, R. L. *Chem. Rev.* **2008**, *108*, 2646−2687.
(50) Li, G.; Jin, R. *Acc. Chem. Res.* **2013**, *46*, 1749−1758.
(51) Mckenzie, L. C.; Zaikova, T. O.; Hutchison, J. E. *J. Am. Chem. Soc.* **2014**, *136*, 13426−13435.
(52) Hicks, J. F.; Zamborini, F. P.; Murray, R. W. *J. Phys. Chem. B* **2002**, *106*, 7751−7757.
(53) Strother, T.; Knickerbocker, T.; Russell, J. N.; Butler, J. E.; Smith, L. M.; Hamers, R. J. *Langmuir* **2002**, *18*, 968−971.
(54) Ilavsky, J.; Jemian, P. R. *J. Appl. Crystallogr.* **2009**, *42*, 347−353.
(55) Yamanoi, Y.; Shirahata, N.; Yonezawa, T.; Terasaki, N.; Yamamoto, N.; Matsui, Y.; Nishio, K.; Masuda, H.; Ikuhara, Y.; Nishihara, H. *Chem. - Eur. J.* **2006**, *12*, 314−323.
(56) Weare, W. W.; Reed, S. M.; Warner, M. G.; Hutchison, J. E. *J. Am. Chem. Soc.* **2000**, *122*, 12890−12891.
(57) Seshan, V.; Ullien, D.; Castellanos-Gomez, A.; Sachdeva, S.; Murthy, D. H. K.; Savenije, T. J.; Ahmad, H. A.; Nunney, T. S.; Janssens, S. D.; Haenen, K.; Nesládek, M.; van der Zant, H. S. J.; Sudhölter, E. J. R.; de Smet, L. C. P. M. *J. Chem. Phys.* **2013**, *138*, 234707.
(58) Nichols, B. M.; Butler, J. E.; Russell, J. N.; Hamers, R. J. *J. Phys. Chem. B* **2005**, *109*, 20938−20947.
(59) Woehrle, G. H.; Hutchison, J. E. *Inorg. Chem.* **2005**, *44*, 6149−6158.
(60) Chidsey, C. E. D.; Bertozzi, C. R.; Putvinski, T. M.; Mujsce, A. M. *J. Am. Chem. Soc.* **1990**, *112*, 4301−4306.
(61) Elliott, E. W.; Glover, R. D.; Hutchison, J. E. *ACS Nano* **2015**, *9*, 3050−3059.
(62) Macpherson, J. V. *Phys. Chem. Chem. Phys.* **2015**, *17*, 2935−2949.
(63) Woehrle, G. H.; Brown, L. O.; Hutchison, J. E. *J. Am. Chem. Soc.* **2005**, *127*, 2172−2183.
(64) Woehrle, G. H.; Warner, M. G.; Hutchison, J. E. *J. Phys. Chem. B* **2002**, *106*, 9979−9981.
(65) Ingram, R. S.; Hostetler, M. J.; Murray, R. W. *J. Am. Chem. Soc.* **1997**, *119*, 9175−9178.
(66) Chazalviel, J.; Allongue, P. *J. Am. Chem. Soc.* **2011**, *133*, 762−764.
(67) Patten, H. V.; Lai, S. C. S.; MacPherson, J. V.; Unwin, P. R. *Anal. Chem.* **2012**, *84*, 5427−5432.
(68) Patten, H. V.; Meadows, K. E.; Hutton, L. A.; Iacobini, J. G.; Battistel, D.; McKelvey, K.; Colburn, A. W.; Newton, M. E.; MacPherson, J. V.; Unwin, P. R. *Angew. Chem., Int. Ed.* **2012**, *51*, 7002−7006.
(69) Ruther, R. E.; Cui, Q.; Hamers, R. J. *J. Am. Chem. Soc.* **2013**, *135*, 5751−5761.
(70) Li, Y.; Huang, W.; Sun, S. *Angew. Chem.* **2006**, *118*, 2599−2601.
(71) Reincke, F.; Hickey, S. G.; Kegel, W. K.; Vanmaekelbergh, D. *Angew. Chem.* **2004**, *116*, 464−468.
(72) Chen, S. *Langmuir* **2001**, *17*, 6664−6668.
(73) Trasatti, S.; Petrii, O. *Pure Appl. Chem.* **1991**, *63*, 711−734.
(74) Wang, X.; Ruther, R. E.; Streifer, J. A.; Hamers, R. J. *J. Am. Chem. Soc.* **2010**, *132*, 4048−4049.
(75) Maat, J. T.; Regeling, R.; Yang, M.; Mullings, M. N.; Bent, S. F.; Zuilhof, H. *Langmuir* **2009**, *25*, 11592−11597.
(76) Franking, R.; Kim, H.; Chambers, S. A.; Mangham, A. N.; Hamers, R. J. *Langmuir* **2012**, *28*, 12085−12093.
(77) Colavita, P. E.; Sun, B.; Tse, K. Y.; Hamers, R. J. *J. Am. Chem. Soc.* **2007**, *129*, 13554−13565.

DOI: 10.1021/jacs.6b07674
J. Am. Chem. Soc. 2016, 138, 13975−13984